



23 **Abstract**

24 Land surface energy and water fluxes play an important role in land-atmosphere interactions,
25 especially for the climatic feedback effects driven by land use/land cover change (LULCC).
26 These have long been documented in model-based studies, but the performance of land surface
27 models in representing LULCC-induced responses has not been well investigated. In this study,
28 measurements from proximate paired (open versus forest) flux tower sites are used to represent
29 observed deforestation-induced changes in surface fluxes, which are compared with simulations
30 from the Community Land Model (CLM) and the Noah Multi-Parameterization (Noah-MP) land
31 model. Point-scale simulations suggest CLM can represent the observed diurnal and seasonal
32 changes in net radiation (R_{net}) and ground heat flux (G), but difficulties remain in the energy
33 partitioning between latent (LE) and sensible (H) heat flux. CLM does not capture the observed
34 decreased daytime LE , and overestimates the increased H during summer. These biases are
35 mainly associated with deficiencies over forest land-cover types and the parameterization of soil
36 evaporation. Global gridded simulations with CLM show uncertainties in the estimation of LE
37 and H at the grid level for regional and global simulations. Noah-MP exhibits a similar ability to
38 simulate the surface flux changes, but with larger biases in H , G , and R_{net} change during late
39 winter and early spring, which are related to a deficiency in estimating albedo. Differences in
40 meteorological conditions between paired sites is not a factor in these results. Attention needs to
41 be devoted to improving the representation of surface heat flux processes in land models to
42 increase confidence in LULCC simulations.

43

44



45 **1. Introduction**

46

47 Earth system models (ESMs) have long been used to investigate the climatic impacts of land
48 use/land cover change (LULCC) (cf. Pielke et al. 2011; Mahmood et al. 2014). Results from
49 sensitivity studies largely depend on the land surface model (LSM) that is coupled to the
50 atmospheric model within ESMs. In the context of the Land-Use and Climate, Identification of
51 Robust Impacts (LUCID) project, Pitman et al. (2009) found disagreement among the LSMs in
52 simulating the LULCC-induced changes in summer latent heat flux over the Northern
53 Hemisphere. de Noblet-Ducoudré et al. (2012) and Boiser et al. (2012) argued that the inter-
54 model spread of LULCC sensitivity (especially regarding the partitioning of available energy
55 between latent and sensible heat fluxes within the different land-cover types) highlights an
56 urgent need for a rigorous evaluation of LSMs. From Phase 5 of the Coupled Model Inter-
57 comparison Project (CMIP5), Brovkin et al. (2013) also found different climatic responses to
58 LULCC among the participating models, which are associated with different parameterizations
59 of land surface processes among ESMs. To deal with the uncertainties in LULCC sensitivity
60 among models, the Land Use Model Inter-comparison Project (LUMIP) has been planned, with a
61 goal to develop metrics and diagnostic protocols that quantify LSM performance and related
62 sensitivities with respect to LULCC (Lawrence et al. 2016).

63

64 However, a paucity of useful observations has hindered the assessment of the simulated impacts
65 of LULCC and limited the understanding of the discrepancies among models. In-situ and satellite
66 observations make it possible to quantify the impacts of LULCC on land surface variables.
67 Satellite-derived datasets have been used to explore the albedo, evapotranspiration (ET), and



68 land surface temperature changes due to historical LULCC (Boisier et al. 2013, 2014) and the
69 climatic effects of forest (Li et al. 2015).

70

71 Meanwhile, the development of FLUXNET (Baldocchi et al. 2001) enables the study of land
72 surface responses to different land-cover types based on paired field observations from
73 neighboring flux towers over forest and open land (Juang et al. 2007; Lee et al. 2011; Luysaert
74 et al. 2014; Teuling et al. 2010; Williams et al. 2012). In terms of LSM evaluation, the paired site
75 observations have been mainly used to simulated impacts of LULCC on land surface temperature
76 (Chen and Dirmeyer 2016; Lejeune et al. 2016; Van den Broucke et al. 2015). However, a more
77 fundamental question, “whether a model can well represent the observed LULCC-induced
78 changes in surface energy fluxes”, has not been thoroughly investigated, even though we know
79 that the turbulent fluxes are tightly associated with both energy and water exchange between the
80 land surface and atmosphere.

81

82 In this study, we evaluate the performance of the Community Land Model (CLM) version 4.5
83 and the Noah Multi-Parameterization (Noah-MP) LSM in simulating the impacts of LULCC on
84 surface energy fluxes based on observations from FLUXNET sites. CLM and Noah-MP
85 represent perhaps the two most readily available and widely used state-of-the-art community
86 land models developed in the U.S. CLM is chosen because, as the land component for
87 Community Earth System Model (CESM), it prioritizes the simulation of biogeophysical and
88 biogeochemical processes for climate applications (Oleson et al. 2013). Much effort has gone
89 into improving the representation of the land-atmosphere interactions among different biomes
90 (Bonan et al. 2011), and the model itself has been used for many LULCC sensitivity studies



91 (e.g., Chen and Dirmeyer 2016, 2017; Schultz et al. 2016; Lejeune et al. 2017; Lawrence et al.
92 2012). Noah-MP has found use mainly in shorter time-scale, limited area applications, such as
93 weather and hydrologic forecasting, and as a LSM run at very high resolution coupled to
94 mesoscale models (e.g., WRF-Hydro, Gochis et al. 2015). It is planned to become the LSM used
95 in global weather and seasonal forecasting applications at the National Centers for
96 Environmental Prediction (NCEP). Its performance over varying land cover types has direct
97 consequences for its use in forecast models.

98

99 The rest of this paper is structured as follows. Section 2 describes the datasets used in the study
100 and experimental design. Section 3 presents comparison between observations and model
101 simulations in surface latent and sensible heat flux, ground heat flux, and net radiation. Section 4
102 shows the uncertainties within the FLUXNET pairs and model simulations. Sections 5 and 6
103 include discussion and conclusions, respectively.

104

105 **2. Methodology**

106

107 *2.1 Observational data*

108

109 We use half-hourly observations from 24 selected pairs of flux sites from the FLUXNET2015
110 Tier 1 dataset (<http://fluxnet.fluxdata.org/data/fluxnet2015-dataset>) and 4 pairs from the
111 AmeriFlux dataset (Baldocchi et al. 2001). These observations include meteorological forcings
112 for the LSM, and surface flux measurements for model validation, which include latent heat flux
113 (LE), sensible heat flux (H), ground heat flux (G), and net radiation (R_{net}). All of these variables



114 have been gap-filled (Reichstein et al. 2005; Vuichard and Papale 2015). Table 1 shows the
115 variable names and gap-filling algorithms used in FLUXNET2015. Because there is no directly
116 measured humidity variable reported, which is needed as a meteorological forcing for the LSMs,
117 relative humidity is calculated based on the reported vapor pressure deficit and surface air
118 temperature (Equation 1-2).

$$e_s = 6.11 \exp\left(17.26938818 \frac{T_a}{237.3 + T_a}\right) \quad (1)$$

$$RH = \left(1 - \frac{VPD}{e_s}\right) \times 100 \quad (2)$$

119 in which T_a is air temperature ($^{\circ}\text{C}$), e_s is saturation vapor pressure (hPa), VPD is vapor pressure
120 deficit (hPa), and RH is relative humidity (%). Additionally, for the turbulent flux measurements
121 over 18 pairs, FLUXNET2015 provides “corrected” fluxes based on an energy balance closure
122 correction factor, which is calculated for each half-hour as $(R_{net} - G) / (H + LE)$. More details
123 about the data processing can be found on the FLUXNET2015 website
124 (<http://fluxnet.fluxdata.org/data/fluxnet2015-dataset/data-processing/>).

125

126 To simulate local land cover change for each pair, one flux tower is located in forest (deciduous,
127 evergreen or mixed; broadleaf or needleleaf) and the other is in a nearby open land cover type
128 (grassland, cropland or open shrub). Figure 1 shows the locations of the paired sites. Their
129 general characteristics are listed in Table S1. The median linear distance between the paired sites
130 is 21.6 km, and the median elevation difference is 20.0 m. Because of their proximities, the
131 paired sites share similar atmospheric background conditions, however they are not identical
132 (Chen and Dirmeyer 2016). Below we show that the differences in meteorology are usually small
133 and not likely a factor in simulated surface flux differences. We consider the differences (open



134 minus forest) in observed surface fluxes to be representative of the effects of LULCC
135 (deforestation in this case).

136

137 *2.2 Model simulations*

138

139 We have run the offline version of CLM 4.5 and Noah-MP at the point-scale for individual sites.
140 The forcing data, described below, includes downwelling long-wave radiation (W/m^2),
141 downwelling short-wave radiation (W/m^2), air temperature (K), precipitation (mm/s), relative
142 humidity (%), surface pressure (Pa), and wind speed (m/s) at half-hourly time steps. The plant
143 functional type (PFT) in CLM for each site is identified based on its reported land cover type
144 (Table S1) with prescribed climatological satellite phenology (Lawrence and Chase, 2010).
145 Because of the focus on biogeophysical impacts of LULCC in this study, the biogeochemistry
146 Carbon-Nitrogen module has been disabled in our simulations. The initial conditions for each
147 site are generated by cycling through available atmospheric forcings for about 40 years until soil
148 moisture and temperature reach quasi-equilibrium.

149

150 The differences in simulated surface fluxes between the paired sites are compared against the
151 observations, so that the performance of CLM in representing LULCC-induced surface flux
152 changes can be evaluated. In the single-point simulations, two types of forcing data are used for
153 each site: 1) measurements at this site; 2) measurements at the neighboring paired site.
154 Consequently, three types of differences in simulated surface fluxes can be calculated: 1) the
155 difference derived from individual forcings; 2) the difference from identical “forest forcings”
156 (both of the paired sites use the same forcings measured at the forest site); 3) the difference from



157 identical “open forcings” (both of the paired sites use the same forcings measured at the open
158 sites). Such an experimental design can well eliminate the influence from the uncertainties of
159 forcing data and the difference in atmospheric background of the paired sites.
160
161 The ultimate goal of evaluating CLM’s performance at single-point scale is to assess its
162 capability to be used in global LULCC sensitivity simulations in both offline and coupled modes.
163 The paired sites are close enough that they are typically located within a single grid cell of
164 CESM. Moreover, the sub-grid heterogeneity of CLM allows the biogeophysical processes to be
165 calculated at the individual PFT level, and makes it possible to output surface fluxes for
166 individual land cover types. The paired sites can be presented as paired PFTs within a single grid
167 of CESM. They then share the same atmospheric forcings, and their differences can be
168 considered as the impacts of LULCC. Therefore, we run CLM offline, globally driven by the
169 CRUNCEP forcings from 1991 to 2010 (Viovy 2011) and present land cover conditions
170 (Lawrence et al. 2012) at a horizontal resolution of $0.9^{\circ} \times 1.25^{\circ}$. The paired PFTs are identified
171 based on the locations and land cover types of the FLUXNET paired sites. Schultz et al. (2016)
172 found the shared-soil-column configuration for vegetated land units in CLM caused issues with
173 PFT-level ground heat fluxes. They propose an individual-soil-column scheme (PFTCOL) to
174 better represent the PFT-level energy fluxes, so we also extract and examine the output for the
175 paired PFTs from the PFTCOL model configuration. Details about the PFTCOL simulations can
176 be found in Schultz et al. (2016). Additionally, a coupled simulation with Community
177 Atmosphere Model (CAM) has also been conducted. It shows very similar results to the offline
178 simulations, because the paired PFTs in a single model grid box always share the same



179 atmospheric forcings no matter if CLM is run offline or coupled with CAM. Therefore, results
180 from the coupled simulation are not included in this study.

181

182 Furthermore, we compare the performance of CLM with Noah-MP (Niu et al. 2011), which
183 serves as a participant model in Land Data Assimilation Systems (LDAS, Cai et al. 2014).
184 Single-point Noah-MP simulations are conducted in the same way as CLM simulations to ensure
185 their comparability. The monthly leaf area index (LAI) of each site is identical to the prescribed
186 satellite-based LAI in the corresponding CLM simulation. Table S2 shows selected options for
187 various physical processes in Noah-MP. Information about all model simulations is summarized
188 in Table 2.

189

190 **3. Surface energy fluxes and their changes**

191

192 First, we analyze the diurnal and seasonal cycles of surface energy fluxes and the LULCC-
193 induced changes. The diurnal cycle analysis is primarily focused on summer (DJF for the two
194 austral sites and JJA for the other sites). The seasonal cycle for the austral sites is shifted by 6
195 months to keep summer in the middle of the time series when comparing or compositing with the
196 Northern Hemisphere sites. The results shown below are composites averaged over all open (or
197 forest) sites or open-forest pairs. Not all sites have energy-balance corrected fluxes available;
198 exclusion of those sites shows very similar results for uncorrected fluxes to the average over all
199 sites (or pairs, not shown). Therefore, all sites without missing variables are included in our
200 analyses for each variable.

201

202 3.1 Latent heat flux (*LE*)

203

204 Figure 2a-b shows the diurnal cycle of *LE* averaged over all the open sites and forest sites during
205 summer. Compared with the observations without energy-balance correction, single-point CLM
206 simulations overestimate *LE* for the open sites with both their actual meteorological forcings and
207 the nearby forest forcings, but underestimate *LE* over the forest sites. The extracted PFT-level
208 output from the global simulations also exhibit similar biases. Relative to CLM, Noah-MP
209 simulations show better agreement with observations over the open sites, but a greater
210 underestimation over forest. The energy-balance correction tends to increase the values of *LE*.
211 Therefore, both CLM and Noah-MP have negative biases compared to the corrected fluxes
212 (except *LE_CORR_25* over the open sites).

213

214 Figure 2c shows the difference in the diurnal cycle of *LE* due to LULCC (deforestation). It
215 should be noted that there is a substantial spread among the pairs in model simulations and
216 especially observations, indicating the diverse geographical backgrounds and specific vegetation
217 changes of these paired sites. The observations suggest an overall lower summer daytime *LE*
218 over the open land compared to forest. In spite of the considerable spread among the energy-
219 balance corrected *LE* observations (Figure 1), the differences between the forest and open lands
220 show consistent signals. However, both CLM and Noah-MP single-point simulations fail to
221 represent the observed decreased daytime *LE* as a result of deforestation. The simulated *LE* over
222 the open land is usually slightly greater than the forest from 10:00 to 16:00 at local time. Such a
223 discrepancy may be attributed to the large underestimation of daytime forest *LE* in the models.
224 Meanwhile, simulations by different forcings of the paired sites show robust signals, implying



225 that the bias of the simulated *LE* sensitivity should not be attributed to the uncertainties of the
226 forcing data. For the CLM global simulations, the PFTCOL case exhibits a similar diurnal
227 pattern to the single-point simulations, while decreased daytime *LE* is found consistently only in
228 the PFT simulations. As CLM-PFT is less physically realistic than CLM-PFTCOL from a soil
229 hydrologic perspective, its superior performance is curious.

230

231 To explore the mechanism of the *LE* changes within CLM, we examine the changes in the three
232 components of evapotranspiration; namely canopy evaporation, canopy transpiration, and ground
233 evaporation (Figure 3). Unfortunately, these separate components are not measured and cannot
234 be directly validated. The CLM, PFT and PFTCOL simulations show an agreement in decreased
235 canopy evaporation after deforestation with the greatest decrease during the early morning.

236 There also is an agreement in an overall decreased canopy transpiration, but CLM simulations do
237 not exhibit an obvious change during the morning when greatly decreased canopy transpiration
238 can be found in the PFT and PFTCOL simulations. The main discrepancy among model versions
239 is found in ground evaporation, which increases after deforestation in the CLM and PFTCOL
240 simulations. The increased ground evaporation has exceeded the decreased canopy evaporation
241 and transpiration, resulting in slightly increased *LE* (Figure 2c). Interestingly, the PFT
242 simulations, which have known issues with PFT-level ground heat flux (Schultz et al. 2016),
243 show decreased daytime ground evaporation. Along with decreased canopy evaporation,
244 transpiration, and ground evaporation, the total *LE* decreases sharply after deforestation in the
245 PFT simulations, which agrees better with the observations than other simulations (Figure 2c).
246 However, the decreased ground evaporation may be associated with a problematic soil-column



247 scheme at sub-grid scale, which undermines the credibility of the agreement between the
248 observations and PFT simulations.
249
250 Figure 4 shows the change in monthly LE after deforestation across the annual cycle. There is
251 clear and consistent seasonality in the LE changes from the observations. The four types of
252 observations show decreased LE (up to -24.0 W/m^2) during local summer. There is little change
253 in LE in the uncorrected observations during the winter season. However, there is significantly
254 increased LE (up to $+17.9 \text{ W/m}^2$) in the energy-balance corrected observations in late winter and
255 early spring. Neither CLM nor Noah-MP capture the observed seasonality of LE change. As
256 found in the change in the diurnal cycle of the LE , the PFTCOL simulations exhibit a similar
257 pattern to the single-point simulations, while the PFT simulations show decreased LE throughout
258 the year with the maximum from May to August, and the best correlation ($R = 0.81$, $P < 0.01$)
259 with observations.

260

261 3.2 Sensible heat flux (H)

262

263 Figure 5a-b shows the diurnal cycle of H averaged over all open and forest sites during local
264 summer. Generally, the models overestimate H throughout the day, with the largest positive bias
265 during midday. Compared with the observations without energy-balance correction, the
266 overestimation can be up to 86.5 W/m^2 from CLM over the forest during noon and 46.4 W/m^2
267 over the open sites. The difference in H between the forest and open sites is shown in Figure 5c
268 Both observations and models exhibit a clear diurnal pattern of change in H after deforestation –
269 a small nighttime increase and a large daytime decrease. Observations show a large spread



270 among the 24 pairs, which is much greater than that from the CLM simulations, indicating
271 uncertainties and variability among the observed fluxes and the robustness of simulated H
272 sensitivity to LULCC in the LSM. Compared with the observations, CLM shows a greater H
273 decrease, which is twice as much as in the observations. The overestimated H decrease may be
274 related to the large positive bias in H over the forest sites (Figure 6). Additionally, the PFT
275 simulations show the largest H decrease, which may be associated with the ground heat issues in
276 the shared-soil-column scheme.

277

278 Seasonally, decreased H is found throughout the year after deforestation in both observations and
279 models (except for the same-forest-forcing CLM simulations in winter, Figure 6). The greatest
280 decrease is observed during spring, when both of the single-point CLM and PFTCOL
281 simulations show good agreement. However, CLM and Noah-MP simulations also show a large
282 decrease during summer, which has not been observed in the FLUXNET dataset. Again, the PFT
283 simulations show the greatest H decrease among the simulations and the largest bias compared
284 with the observations during the warm season.

285

286 *3.3 Diurnal and seasonal cycle of ground heat flux (G) and net radiation (R_{net})*

287

288 Figure 7 shows the change in the diurnal cycle of G after deforestation. Both the observations
289 and models exhibit increased G during the day and decreased G during the night. However,
290 models overestimate the magnitude of the G change, and discrepancies also exist in the timing of
291 maximum change. The greatest increase in G is observed during early afternoon, while the
292 greatest increase in simulated G occurs at noon in CLM (single-point and PFTCOL) and during



293 morning in Noah-MP. Because G is strongly correlated with R_{net} (Santanello and Friedl 2003),
294 we examine the timing of maximum observed G and R_{net} during summer. There are some sites
295 showing about 1-hour lag between maximum R_{net} and G (not shown). Therefore, the lag between
296 simulated and observed peaks in G change can be partially attributed to the uncertainties in G
297 measurements that are commonly estimated with heat flux plates installed at some depth (e.g.,
298 5~10 cm) below the surface (Wang and Bou-Zeid 2012), while the LSM simulated G is
299 calculated at the surface. Meanwhile, the G changes (in both the diurnal and seasonal cycle) in
300 the PFT simulations are further from the observations than the other simulations. Such
301 disagreement further confirms the issues with the sub-grid soil column scheme in CLM, which is
302 discussed in the following section. The changes in observed G also have a clear seasonal pattern
303 – an increase during the warm season and a decrease during the cold season. This seasonality is
304 well captured by the CLM simulations (especially the simulations with identical forcings for the
305 paired sites) in both magnitude and timing, but not evident in Noah-MP simulations (Figure 8).
306

307 After exploring the three flux components of the surface energy balance, it is worthwhile to
308 examine the change in R_{net} after deforestation. During summer, the observations show that R_{net}
309 slightly increases during the night, and decreases considerably (up to -65.7 W/m^2) during the
310 day, which can be attributed to the increased albedo after deforestation (Figure 9). Decreased
311 daytime R_{net} is also found in the CLM simulations, but with a slightly smaller magnitude.
312 Seasonally, there is a good agreement between the observations and CLM simulations, showing
313 a large R_{net} decrease during spring and summer but a relatively small decrease during autumn and
314 winter (Figure 10). The Noah-MP simulations are comparable to CLM, but with a notable
315 deficiency in simulating the R_{net} change during late winter and early spring.



316

317 **4. Uncertainty Analysis**

318

319 *4.1 Uncertainties among the FLUXNET pairs*

320

321 The results discussed above are based on composites averaged over all forest and open sites. It is
322 worthwhile to examine the uncertainties in surface flux changes among different paired sites.

323 Figure 11a shows the changes in summer daytime (8:00 ~ 16:00) *LE* from the observations and

324 model simulations across the 28 pairs. This time period is chosen because it is the time of

325 greatest differences in surface energy fluxes (Figure 2c, 5c, 7, 9). The observations show

326 decreased *LE* associated with deforestation over 23 pairs, among which the pairs of evergreen

327 needleleaf forest and open shrub (No. 16~25) exhibit consistent decreases and the pairs of

328 deciduous broadleaf forest and crops (No. 1~4) show the overall greatest decrease. However,

329 both CLM and Noah-MP show relatively weak increases over most of the pairs, which further

330 demonstrates their deficiency in simulating *LE* change. Additionally, for both CLM or Noah, the

331 choice of forcings does not exert much influence on the simulated change in summer daytime

332 *LE*.

333

334 The changes in R_{net} over individual pairs are shown in Figure 11b. There are 27 pairs (all except

335 number 21) showing decreased R_{net} after deforestation, with the greatest decreases over the pairs

336 of evergreen needleleaf forest and grassland. Both CLM and Noah-MP well captures the

337 observed decreases in R_{net} over most of the pairs.

338



339 It should be noted that pair 15 shows large LE and R_{net} changes in Figure 11. This pair consists of
340 a site over valley grassland and the other site over mountain evergreen needleleaf forest with
341 60.29 km separation and 1186 m elevation difference. There are significantly different air
342 temperature and downwelling longwave radiation measurements between the sites (Figure S1).
343 Such large differences in LE and R_{net} here are likely associated with the distinct geographical
344 sites. Even though the exclusion of this site does not make a significant change to the composite
345 analysis in section 3 (not shown), it may raise another question if the simulated sensitivity of
346 surface energy fluxes is associated with the uncertainties of atmospheric forcings of LSMs at the
347 single pair level.

348

349 *4.2 Uncertainties within the forcings for LSMs*

350

351 Based on the composite analysis in section 3, we have found that the simulated changes in
352 surface energy fluxes with identical forcings (either from forest or open sites) are consistent with
353 the simulations with individual forcings, demonstrating that the overall sensitivities of surface
354 energy fluxes are robust among the choices of different forcings. In this sub-section, we explore
355 the uncertainties of the simulated surface flux changes due to the different forcings for individual
356 pairs, especially with the focus on the roles of separation and elevation difference in the
357 simulated sensitivity of surface energy fluxes.

358

359 Since we have simulations with identical forcings for the paired sites, the difference in surface
360 flux changes between “forest forcings” and “open forcings” can be considered as the simulated
361 sensitivity of surface energy fluxes to variation in the atmospheric forcings. Figure 12 shows the



362 relationship with separation and elevation difference for individual pairs. Overall, the flux
363 changes are not associated with the separation and elevation difference between the paired sites,
364 further confirming the robustness of simulated signals from paired-site simulations.
365 Nevertheless, some “outliers” are identified. In the CLM simulations, only pair 15 shows large
366 differences in LE and H change. However, pairs 3, 7, and 12 also exhibit large differences in
367 Noah-MP simulations. The uncertainties in pairs 12 and 15 may be attributed to their large
368 elevation differences. For pair 7 in Australia, Noah-MP shows greater sensitivity of H and R_{net} to
369 atmospheric forcings over the evergreen broadleaf forest than grassland (not shown), leading to
370 large differences in the surface flux changes. However, this is the only pair with evergreen
371 broadleaf forest, and its behavior in Noah-MP needs further investigation. Even though the pair 3
372 sites are close with small elevation difference, we found considerably different downwelling
373 shortwave and longwave radiation between the two sites (not shown), which may explain the
374 uncertainties in the Noah-MP simulations.

375

376 5. Discussion

377

378 This study has examined simulated changes in the surface energy budget in response to local
379 land cover change based on paired proximate FLUXNET sites with differing land cover. Our
380 results suggest that CLM well represents the observed changes in R_{net} and G ; but there remain
381 issues in simulating the energy partitioning between LE and H , which also further confirms the
382 large uncertainties in simulated ET responses to LULCC revealed in several recent studies (e.g.,
383 Pitman et al. 2009; Boisier et al. 2012, 2014; de Noblet-Ducoudré et al. 2012; Van den Broucke
384 et al. 2015). Based on the observations, deforestation generally leads to a decrease in summer



385 daytime R_{net} , accompanied by decreased LE and H . On one hand, CLM captures the observed
386 signal of H change, but overestimates the decrease due to its large overestimation of H over the
387 forest. On the other hand, the model underestimates the LE over the forest, leading to an opposite
388 signal (a slight increase) of LE change comparing to the observations. Simulations in Noah-MP
389 show similar biases. Therefore, uncertainties in current LULCC sensitivity studies may persist
390 specifically in the representation of turbulent fluxes over forest land-cover types.

391

392 Scrutinizing the three components of ET suggests that the simulated increase in summer daytime
393 LE is mainly attributable to a large increase in ground evaporation, which counteracts the
394 decreased canopy evaporation and transpiration. This may raise another issue about the soil
395 resistance parameterization in CLM4.5. Previous studies indicate that the model generates
396 excessive ground evaporation when the canopy is sparse or absent (Swenson and Lawrence
397 2014; Tang et al. 2015). If there is overestimated ground evaporation over the open land, such a
398 bias can also contribute to the disagreement in the LULCC-induced ET changes. Swenson and
399 Lawrence (2014) have implemented a dry surface layer for the soil resistance parameterization to
400 solve this issue for the upcoming CLM5. An extension of the evaluation with CLM5 would be
401 useful to examine if the issue within the soil resistance parameterization is responsible for the
402 uncertainties in ET changes.

403

404 Besides the uncertainties in estimating turbulent fluxes over different land cover types, the
405 simulations show that differences in the meteorological forcings between nearby paired sites
406 seem to have little impact on the simulation of surface flux changes due to LULCC. Many
407 LSMs besides CLM employ a sub-grid tiling parameterization where multiple land surface types



408 exist within a single grid box, each maintaining a separate set of surface balances and returning a
409 weighted average set of fluxes to the atmosphere based on areal coverage of each surface type.
410 In this arrangement, each land surface type within a grid box receives the same meteorological
411 forcing from the overlying atmospheric model. It appears from our forcing-sensitivity studies
412 that this arrangement does not significantly impact the simulation of surface flux changes
413 associated with LULCC on the grid scale.

414

415 That said, the sub-grid comparison between different land cover types may yet be problematic
416 due to the shared soil column issue for vegetated land units in CLM (Schultz et al. 2016). Both
417 the single-point observations and simulations show significant differences in surface soil
418 moisture between most of the paired sites, even though no clear drying or wetting pattern is
419 found (Figure S2). The differences between the paired sites suggests that the shared soil column
420 for vegetated land in CLM may not well represent soil moisture and temperature at the sub-grid
421 scale, which may influence the simulations of land surface energy and water fluxes. We find an
422 unreasonably large change in PFT-level G between forest and open land especially for the
423 seasonal cycle in PFT simulations, while both observations, single-point and PFTCOL
424 simulations show a seasonal change with a very small range (within $\pm 3\text{W/m}^2$). As G is the
425 calculated as the residual of the surface energy budget in CLM (Oleson et al. 2013), this sub-grid
426 G issue may cast even more uncertainties on the calculation of LE and H at the PFT level, as well
427 as their aggregated values at the grid level for regional or global simulations. Therefore, caution
428 should be taken when examining the LULCC sensitivity which involves sub-grid PFT changes.

429



430 Compared with CLM, Noah-MP exhibits a similar ability to simulate surface flux changes,
431 except for the deficiency in simulating H and R_{net} changes during late winter and early spring.
432 We have examined the daytime albedo change after deforestation, calculated from available
433 shortwave radiation terms, from observations and model simulations during local late
434 winter/early spring (February ~ April, FMA) and summer (Figure 13). Both CLM and Noah-MP
435 agree with the observations during summer. However, Noah-MP does not capture the observed
436 albedo increase over nearly half of the pairs during late winter/early spring. Greater disagreement
437 is also found during the local winter season (DJF, not shown), suggesting a deficiency in
438 snowmelt timing or snow albedo sensitivity to LULCC, despite improvement in the snow surface
439 albedo simulations by implementation of the Canadian Land Surface Scheme (CLASS;
440 Verseghy, 1991) in Noah-MP (Niu et al. 2011).

441

442 Finally, it should be recognized that the observational data are not perfect. In particular, there
443 may be systematic biases or even trends in specific instruments that contribute to the perceived
444 differences between paired sites (e.g., site 3). Ideally, redundant instrumentation at sites, or in
445 this case the rotation of an extra set of instruments among nearby paired sites, could be used to
446 identify, quantify and account for significant systematic biases in measurements for suspicious
447 variables.

448

449 **5. Conclusions**

450

451 This study has evaluated the performance of two state-of-the-art LSMs in simulating the
452 LULCC-induced changes in surface energy fluxes. Observations from 28 FLUXNET pairs (open



453 versus forest) are used to represent the observed flux changes following deforestation, which are
454 compared with the LSM simulations forced with meteorological data from the observation sites.
455 Diurnal and seasonal cycles of the flux changes have been investigated.

456

457 The single-point simulations in CLM and Noah-MP show the greatest bias in simulating *LE*
458 change. Significantly decreased daytime *LE* is observed during local summer, but not captured
459 by the models. The observed *LE* changes also exhibit an evident seasonality, which is not
460 represented in the model. The energy partitioning between *LE* and *H* might be a common issue
461 within the LSMs. Other studies have noted problems in the simulation of surface fluxes by
462 LSMs, including poor performance relative to non-physical statistical models (Best et al. 2015,
463 Haughton et al. 2016).

464

465 The sub-grid comparison from the global simulations in CLM yields unrealistic changes in *G* and
466 *H* when the soil column is shared among vegetated land units, even though there is a better
467 agreement in *LE* change with the observations. The individual-soil-column scheme improves the
468 representation of the PFT-level energy flux changes, but uncertainties still remain as with the
469 point-scale simulations. Therefore, these uncertainties must be considered when interpreting
470 global experiments of LULCC sensitivity studies with current LSMs.

471

472 Consistent aggregate performance across many paired sites suggests the problems in these LSMs
473 may not lie primarily with parameter selection at individual sites, but with more fundamental
474 issues of the representation of physical processes in LSMs. The simulation of LULCC may or
475 may not have become more consistent among models since LUCID (de Noblet-Ducoudré et al.



476 2012), but consistency with observed biophysical responses appears to be lacking. LUMIP
477 (Lawrence et al. 2016) will be a step toward better LSM simulation of LULCC responses, and
478 ultimately better simulations of the response of climate to LULCC.

479

480

481

482 *Acknowledgements:*

483 This study was supported by the National Science Foundation (AGS-1419445). This work used
484 eddy covariance data acquired and shared by the FLUXNET community, including these
485 networks: AmeriFlux, CarboEuropeIP, CarboItaly, CarboMont, Fluxnet-Canada, GreenGrass,
486 ICOS, and OzFlux-TERN. The ERA-Interim reanalysis data are provided by ECMWF and
487 processed by LSCE. The FLUXNET eddy covariance data processing and harmonization was
488 carried out by the European Fluxes Database Cluster, AmeriFlux Management Project, and
489 Fluxdata project of FLUXNET, with the support of CDIAC and ICOS Ecosystem Thematic
490 Center, and the OzFlux, ChinaFlux and AsiaFlux offices. We thank all site investigators and flux
491 networks for their work to make our model evaluation possible. The authors wish to thank
492 Ahmed Tawfik at the National Center for Atmospheric Research for his assistance of preparing
493 forcing datasets for the AmeriFlux sites. Computing resources for the CLM and Noah-MP
494 experiments were provided by the NSF/CISL/Yellowstone supercomputing facility.

495

496

497

498



499

REFERENCES

500

501 Baldocchi, D. and Coauthors, 2001: FLUXNET: A New Tool to Study the Temporal and Spatial
502 Variability of Ecosystem–Scale Carbon Dioxide, Water Vapor, and Energy Flux
503 Densities. *Bull. Amer. Meteor. Soc.*, **82**, 2415-2434, doi:10.1175/1520-
504 0477(2001)082<2415:FANTTS>2.3.CO;2.

505 Betts, A. K., 2004: Understanding Hydrometeorology Using Global Models. *Bull. Amer. Meteor.*
506 *Soc.*, **85**, 1673-1688, doi:10.1175/BAMS-85-11-1673.

507 Boisier, J., N. de Noblet-Ducoudré, and P. Ciais, 2014: Historical land-use-induced
508 evapotranspiration changes estimated from present-day observations and reconstructed
509 land-cover maps. *Hydrology and Earth System Sciences*, **18**, 3571-3590,

510 Boisier, J., N. de Noblet-Ducoudré, and P. Ciais, 2013: Inferring past land use-induced changes
511 in surface albedo from satellite observations: a useful tool to evaluate model
512 simulations. *Biogeosciences*, **10**, 1501-1516,

513 Boisier, J. P. and Coauthors, 2012: Attributing the impacts of land-cover changes in temperate
514 regions on surface temperature and heat fluxes to specific causes: Results from the first
515 LUCID set of simulations. *Journal of Geophysical Research: Atmospheres*, **117**, n/a-n/a,
516 doi:10.1029/2011JD017106.

517 Bright, R. M., K. Zhao, R. B. Jackson, and F. Cherubini, 2015: Quantifying surface albedo and
518 other direct biogeophysical climate forcings of forestry activities. *Global Change*
519 *Biol.*, **21**, 3246-3266, doi:10.1111/gcb.12951.



- 520 Brovkin, V. and Coauthors, 2013: Effect of Anthropogenic Land-Use and Land-Cover Changes
521 on Climate and Land Carbon Storage in CMIP5 Projections for the Twenty-First
522 Century. *J. Climate*, **26**, 6859-6881, doi:10.1175/JCLI-D-12-00623.1.
- 523 Cai, X., Z. Yang, Y. Xia, M. Huang, H. Wei, L. R. Leung, and M. B. Ek, 2014: Assessment of
524 simulated water balance from Noah, Noah-MP, CLM, and VIC over CONUS using the
525 NLDAS test bed. *Journal of Geophysical Research: Atmospheres*, **119**, 13,751-13,770,
526 doi:10.1002/2014JD022113.
- 527 Chen, L., and P. A. Dirmeyer, 2016: Adapting observationally based metrics of biogeophysical
528 feedbacks from land cover/land use change to climate modeling. *Environmental Research
529 Letters*, **11**, 034002,
- 530 Chen, L., and P. A. Dirmeyer, 2016: Impacts of Land Use/Land Cover Change on Afternoon
531 Precipitation over North America. *J. Climate*, doi:10.1175/JCLI-D-16-0589.1.
- 532 de Noblet-Ducoudré, N. and Coauthors, 2012: Determining Robust Impacts of Land-Use-
533 Induced Land Cover Changes on Surface Climate over North America and Eurasia:
534 Results from the First Set of LUCID Experiments. *J. Climate*, **25**, 3261-3281,
535 doi:10.1175/JCLI-D-11-00338.1.
- 536 Dirmeyer, P. A., R. D. Koster, and Z. Guo, 2006: Do Global Models Properly Represent the
537 Feedback between Land and Atmosphere? *J. Hydrometeor.*, **7**, 1177-1198,
538 doi:10.1175/JHM532.1.



- 539 Foken, T., 2008: THE ENERGY BALANCE CLOSURE PROBLEM: AN OVERVIEW. *Ecol.*
540 *Appl.*, **18**, 1351-1367, doi:10.1890/06-0922.1.
- 541 Gochis, D.J., W. Yu, and D.N. Yates, 2015. The WRF-Hydro Model Technical Description and
542 User's Guide, Version 3.0. NCAR Technical Document, 120 pp., [Available at
543 [https://www.ral.ucar.edu/sites/default/files/public/images/project/WRF_Hydro_User_Gui](https://www.ral.ucar.edu/sites/default/files/public/images/project/WRF_Hydro_User_Guide_v3.0.pdf)
544 [de_v3.0.pdf](https://www.ral.ucar.edu/sites/default/files/public/images/project/WRF_Hydro_User_Guide_v3.0.pdf)].
- 545 Janowiak, J. E., V. E. Kousky, and R. J. Joyce, 2005: Diurnal cycle of precipitation determined
546 from the CMORPH high spatial and temporal resolution global precipitation
547 analyses. *Journal of Geophysical Research: Atmospheres*, **110**, n/a-n/a,
548 doi:10.1029/2005JD006156.
- 549 Juang, J., G. Katul, M. Siqueira, P. Stoy, and K. Novick, 2007: Separating the effects of albedo
550 from eco-physiological changes on surface temperature along a successional
551 chronosequence in the southeastern United States. *Geophys. Res. Lett.*, **34**, n/a-n/a,
552 doi:10.1029/2007GL031296.
- 553 Lawrence, D. M. and Coauthors, 2016: The Land Use Model Intercomparison Project (LUMIP)
554 contribution to CMIP6: rationale and experimental design. *Geoscientific Model*
555 *Development*, **9**, 2973-2998,
- 556 Lawrence, D., and K. Vandecar, 2015: Effects of tropical deforestation on climate and
557 agriculture. *Nature climate change*, **5**, 27-36,



- 558 Lawrence, P. J., and T. N. Chase, 2010: Investigating the climate impacts of global land cover
559 change in the community climate system model. *Int. J. Climatol.*, **30**, 2066-2087,
560 doi:10.1002/joc.2061.
- 561 Lawrence, P. J. and Coauthors, 2012: Simulating the Biogeochemical and Biogeophysical
562 Impacts of Transient Land Cover Change and Wood Harvest in the Community Climate
563 System Model (CCSM4) from 1850 to 2100. *J. Climate*, **25**, 3071-3095,
564 doi:10.1175/JCLI-D-11-00256.1.
- 565 Lee, X. and Coauthors, 2011: Observed increase in local cooling effect of deforestation at higher
566 latitudes. *Nature*, **479**, 384-387, doi: 10.1038/nature10588.
- 567 Lejeune, Q., S. I. Seneviratne, and E. L. Davin, 2016: Historical land-cover change impacts on
568 climate: comparative assessment of LUCID and CMIP5 multi-model experiments. *J.*
569 *Climate*, doi:10.1175/JCLI-D-16-0213.1.
- 570 Li, Y., M. Zhao, S. Motesharrei, Q. Mu, E. Kalnay, and S. Li, 2015: Local cooling and warming
571 effects of forests based on satellite observations. *Nature communications*, **6**, doi:
572 10.1038/ncomms7603.
- 573 Luysaert, S. and Coauthors, 2014: Land management and land-cover change have impacts of
574 similar magnitude on surface temperature. *Nature Climate Change*, **4**, 389-393, doi:
575 10.1038/nclimate2196.
- 576 Mahmood, R. and Coauthors, 2014: Land cover changes and their biogeophysical effects on
577 climate. *Int. J. Climatol.*, **34**, 929-953, doi:10.1002/joc.3736.



- 578 Niu, G. and Coauthors, , 2011: The community Noah land surface model with
579 multiparameterization options (Noah-MP): 1. Model description and evaluation with
580 local-scale measurements. *Journal of Geophysical Research: Atmospheres*, **116**, D12109,
581 doi:10.1029/2010JD015139.
- 582 Oleson, K. W., and co-authors, 2013: Technical Description of version 4.5 of the Community
583 Land Model (CLM), NCAR Technical Note, TN-503+STR, National Center for
584 Atmospheric Research, Boulder, CO, USA, 434pp., [Available at
585 http://www.cesm.ucar.edu/models/cesm1.2/clm/CLM45_Tech_Note.pdf].
- 586 Pielke, R. A. and Coauthors, , 2011: Land use/land cover changes and climate: modeling analysis
587 and observational evidence. *Wiley Interdisciplinary Reviews: Climate Change*, **2**, 828-
588 850, doi:10.1002/wcc.144.
- 589 Pitman, A. J. and Coauthors, , 2009: Uncertainties in climate responses to past land cover
590 change: First results from the LUCID intercomparison study. *Geophys. Res. Lett.*, **36**, n/a-
591 n/a, doi:10.1029/2009GL039076.
- 592 Portmann, F. T., S. Siebert, and P. Döll, 2010: MIRCA2000—Global monthly irrigated and
593 rainfed crop areas around the year 2000: A new high-resolution data set for agricultural
594 and hydrological modeling. *Global Biogeochem. Cycles*, **24**, L14814,
595 doi:10.1029/2008GB003435.
- 596 Reichstein, M. and Coauthors, , 2005: On the separation of net ecosystem exchange into
597 assimilation and ecosystem respiration: review and improved algorithm. *Global Change*
598 *Biol.*, **11**, 1424-1439, doi:10.1111/j.1365-2486.2005.001002.x.



- 599 Santanello, J. A., and M. A. Friedl, 2003: Diurnal Covariation in Soil Heat Flux and Net
600 Radiation. *J. Appl. Meteor.*, **42**, 851-862, doi:10.1175/1520-
601 0450(2003)042<0851:DCISHF>2.0.CO;2.
- 602 Schultz, N. M., X. Lee, P. J. Lawrence, D. M. Lawrence, and L. Zhao, 2016: Assessing the use
603 of subgrid land model output to study impacts of land cover change. *Journal of*
604 *Geophysical Research: Atmospheres*, **121**, 6133-6147, doi:10.1002/2016JD025094.
- 605 Swenson, S. C., and D. M. Lawrence, 2014: Assessing a dry surface layer-based soil resistance
606 parameterization for the Community Land Model using GRACE and FLUXNET-MTE
607 data. *Journal of Geophysical Research: Atmospheres*, **119**, 10,299-10,312,
608 doi:10.1002/2014JD022314.
- 609 Tang, J., W. J. Riley, and J. Niu, 2015: Incorporating root hydraulic redistribution in CLM4.5:
610 Effects on predicted site and global evapotranspiration, soil moisture, and water
611 storage. *Journal of Advances in Modeling Earth Systems*, **7**, 1828-1848,
612 doi:10.1002/2015MS000484.
- 613 Teuling, A. J. and Coauthors, 2010: Contrasting response of European forest and grassland
614 energy exchange to heatwaves. *Nature Geoscience*, **3**, 722-727, doi:10.1038/ngeo950.
- 615 Verseghy, D. L., 1991: Class—A Canadian land surface scheme for GCMS. I. Soil model. *Int. J.*
616 *Climatol.*, **11**, 111-133, doi:10.1002/joc.3370110202.
- 617 Viovy, N., 2011. CRUNCEP data set for 1901–2008, [Available at
618 <https://www.earthsystemgrid.org/dataset/ucar.cgd.cesm4.CRUNCEP.v4.html>].



- 619 Vuichard, N., and D. Papale, 2015: Filling the gaps in meteorological continuous data measured
620 at FLUXNET sites with ERA-Interim reanalysis. *Earth System Science Data*, **7**, 157-171,
621 doi:10.5194/essd-7-157-2015.
- 622 Williams, C. A. and Coauthors, 2012: Climate and vegetation controls on the surface water
623 balance: Synthesis of evapotranspiration measured across a global network of flux
624 towers. *Water Resour. Res.*, **48**, W06523, doi:10.1029/2011WR011586.
- 625 Wilson, K. and Coauthors, 2002: Energy balance closure at FLUXNET sites. *Agric. For.*
626 *Meteorol.*, **113**, 223-243, doi:10.1016/S0168-1923(02)00109-0.
- 627 Xu, Z., R. Mahmood, Z. Yang, C. Fu, and H. Su, 2015: Investigating diurnal and seasonal
628 climatic response to land use and land cover change over monsoon Asia with the
629 Community Earth System Model. *Journal of Geophysical Research: Atmospheres*, **120**,
630 1137-1152, doi:10.1002/2014JD022479.
- 631 Zhang, L. and Coauthors, , 2016: Evaluation of the Community Land Model simulated carbon
632 and water fluxes against observations over ChinaFLUX sites. *Agric. For. Meteorol.*, **226–**
633 **227**, 174-185, doi:10.1016/j.agrformet.2016.05.018.
- 634
- 635
- 636
- 637
- 638
- 639



640 **Table 1.** Information about the variables used from FLUXNET2015. The marginal distribution
641 sampling (MDS) filling method is based on Reichstein et al. (2005); and the ERA-interim filling
642 method can be found in Vuichard and Papale (2015).

Name	Gap-filling	Description
SW_IN_F	MDS and ERA-interim	downwelling shortwave radiation
LW_IN_F	MDS and ERA-interim	downwelling longwave radiation
PA_F	MDS and ERA-interim	atmospheric pressure
TA_F	MDS and ERA-interim	air temperature
VPD_F	MDS and ERA-interim	vapor pressure deficit
P_F	ERA-interim	precipitation
WS_F	ERA-interim	wind speed
LE_F_MDS	MDS	latent heat flux
H_F_MDS	MDS	sensible heat flux
G_F_MDS	MDS	ground heat flux
NETRAD	n/a	net radiation
LE_CORR	n/a	corrected LE_F_MDS by energy balance closure correction factors. LE_CORR_25, LE_CORR, and LE_CORR_75 are calculated based on 25, 50, and 75th percentiles of the factors, respectively.
H_CORR	n/a	corrected H_F_MDS by energy balance closure correction factors. H_CORR_25, H_CORR, and H_CORR_75 are calculated based on 25, 50, and 75th percentiles of the factors, respectively.

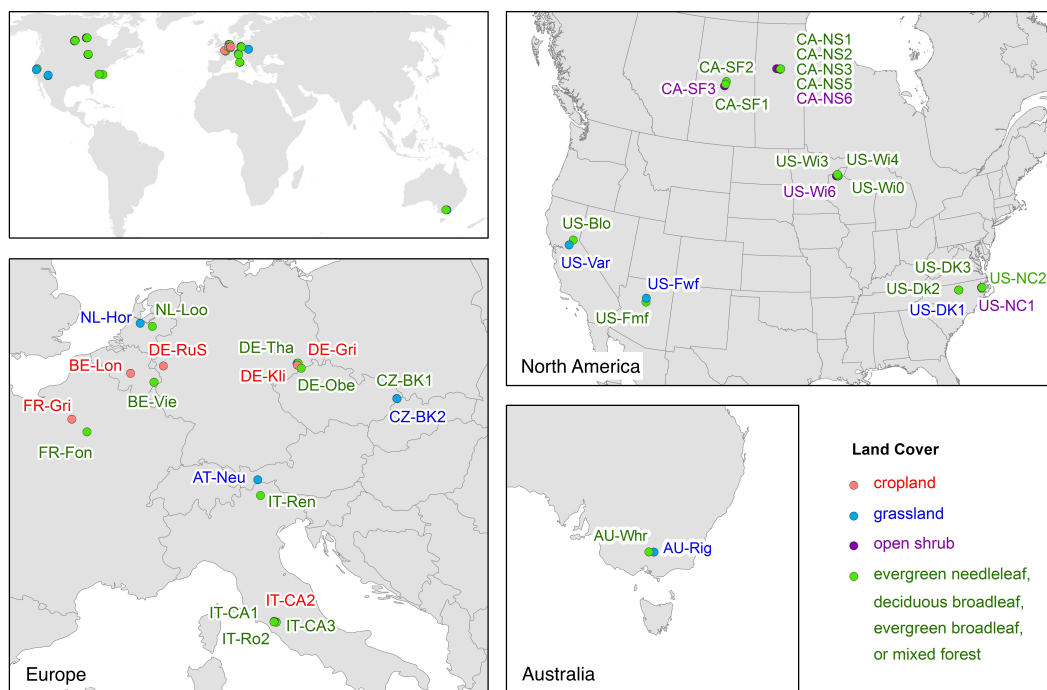
643
644
645
646



647 **Table 2.** Information about model simulations. “Nearby” observations indicate that the paired
 648 sites have the identical forcings either from the companion forest or open sites.

Name	Forcings	Description
CLM	observations from individual sites	single-point CLM simulations with its own observations
CLM_forest	observations only from forest sites	single-point CLM simulations with the (nearby) forest observations
CLM_open	observations only from open sites	single-point CLM simulations with the (nearby) open land observations
CLM-PFT	CRUNCEP	global CLM simulations with default soil-column scheme with PFT-level output
CLM-PFTCOL	CRUNCEP	global CLM simulations with default individual-soil-column scheme scheme with PFT-level output
NOAH-MP	observations from individual sites	single-point NOAH-MP simulations with its own observations
NOAH-MP_forest	observations only from forest sites	single-point NOAH-MP simulations with the (nearby) forest observations
NOAH-MP_open	observations only from open sites	single-point NOAH-MP simulations with the (nearby) open land observations

649
 650
 651
 652
 653
 654
 655
 656



657

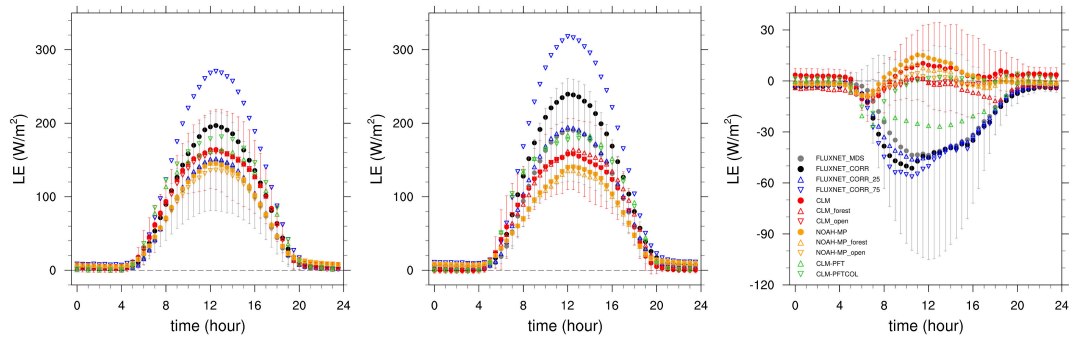
658 **Figure 1.** Location and land cover type of the paired sites.

659

660

661

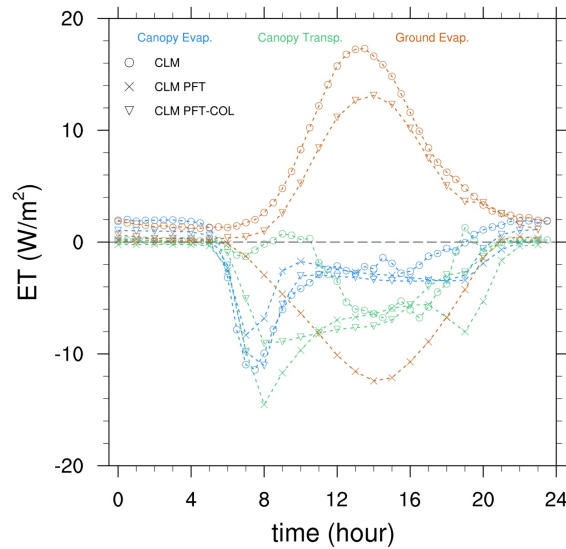
662



663

664 **Figure 2.** The diurnal cycle of LE (W/m^2) averaged over all the open sites (a) and forest sites (b)
 665 and their difference (c) during the summer. The gray error bars indicate the standard deviation of
 666 the observed LE (MDS) among the sites; the red error bars are for the simulated LE in the CLM
 667 case. Details about the four types of FLUXNET observations can be found in Table . Information
 668 about model simulations in CLM and Noah is described in Table 2.

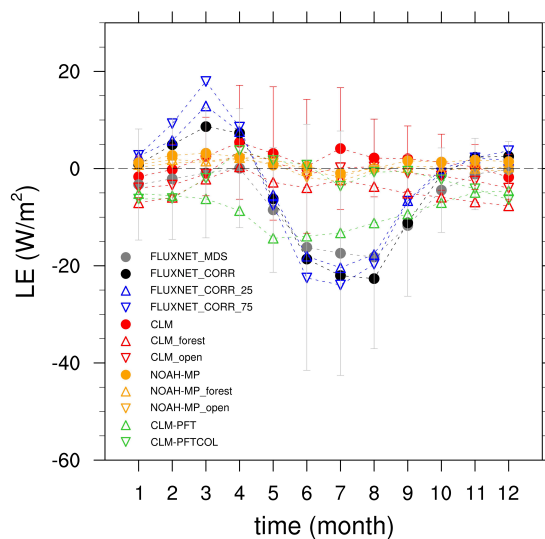
669



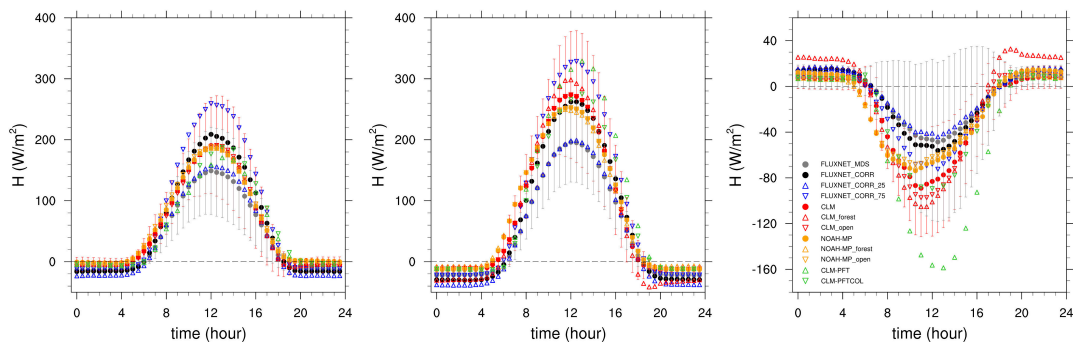
670



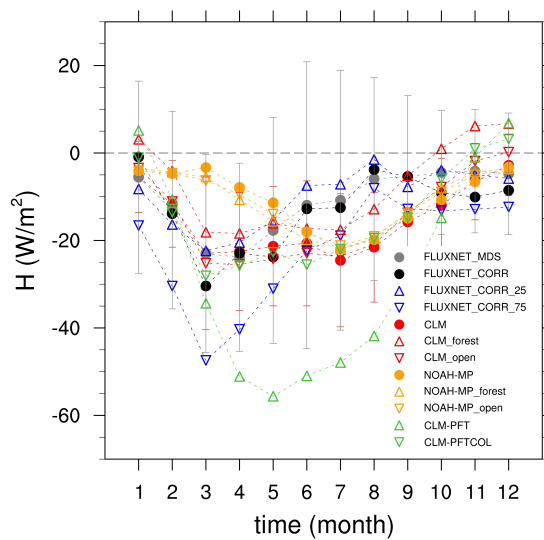
671 **Figure 3.** Change in the diurnal cycle of components (colors) of evapotranspiration (canopy
 672 evaporation, canopy transpiration, and ground evaporation) due to LULCC from forest to open
 673 land.



674
 675 **Figure 4.** Change in the seasonal cycle of LE (W/m^2) due to LULCC from forest to open land.
 676
 677



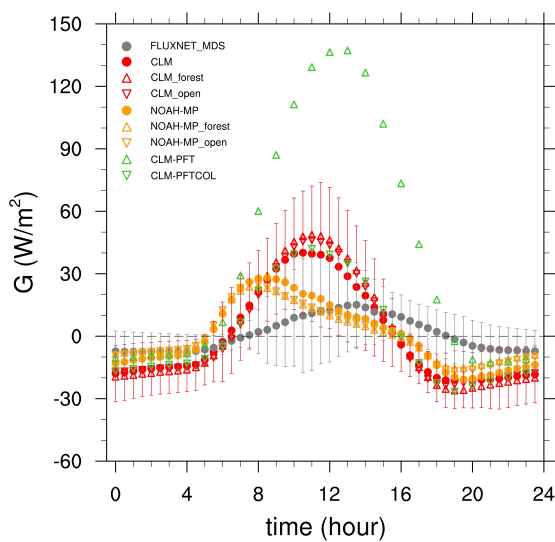
678
 679 **Figure 5.** Same as Figure 2 but for H (W/m^2).
 680



681

682 **Figure 6.** Same as Figure 4 but for H (W/m^2).

683

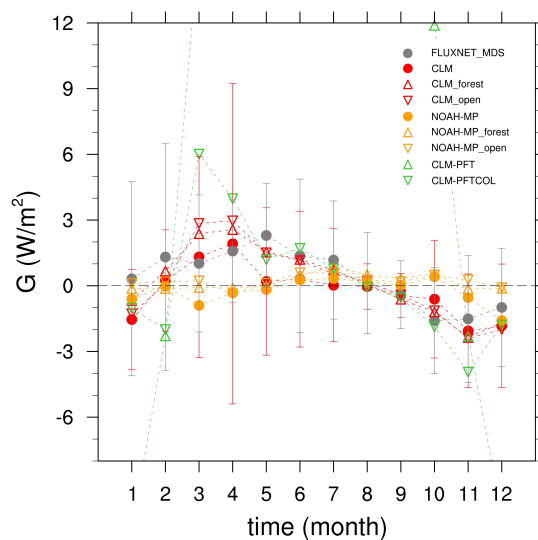


684

685

686 **Figure 7.** Same as Figure 2c but for G (W/m^2).

687

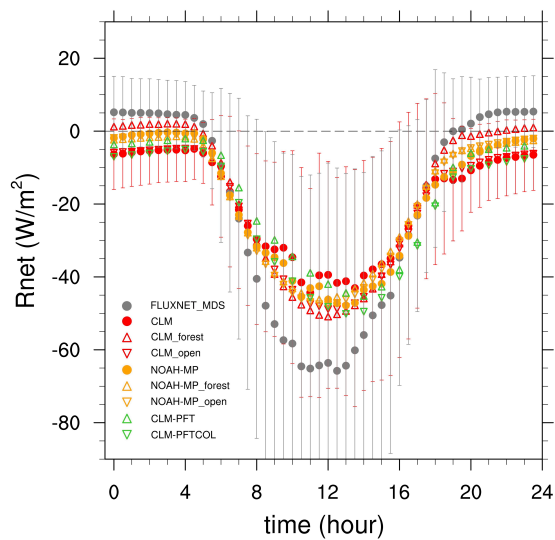


688

689 **Figure 8.** Same as Figure 4 but for G (W/m^2). It should be noted that the changes in the CLM-
690 PFT simulation are much further from the observations than the other simulations. Some of its
691 values are beyond the limit of the figure. The smallest value is $-11.2 \text{ W}/\text{m}^2$ in January; while the
692 largest value is $52.9 \text{ W}/\text{m}^2$ in May.

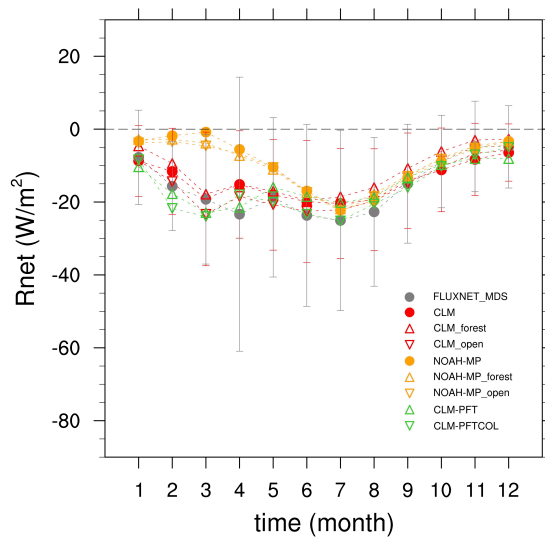
693

694



695

696 **Figure 9.** Same as Figure 2c but for R_{net} (W/m^2).

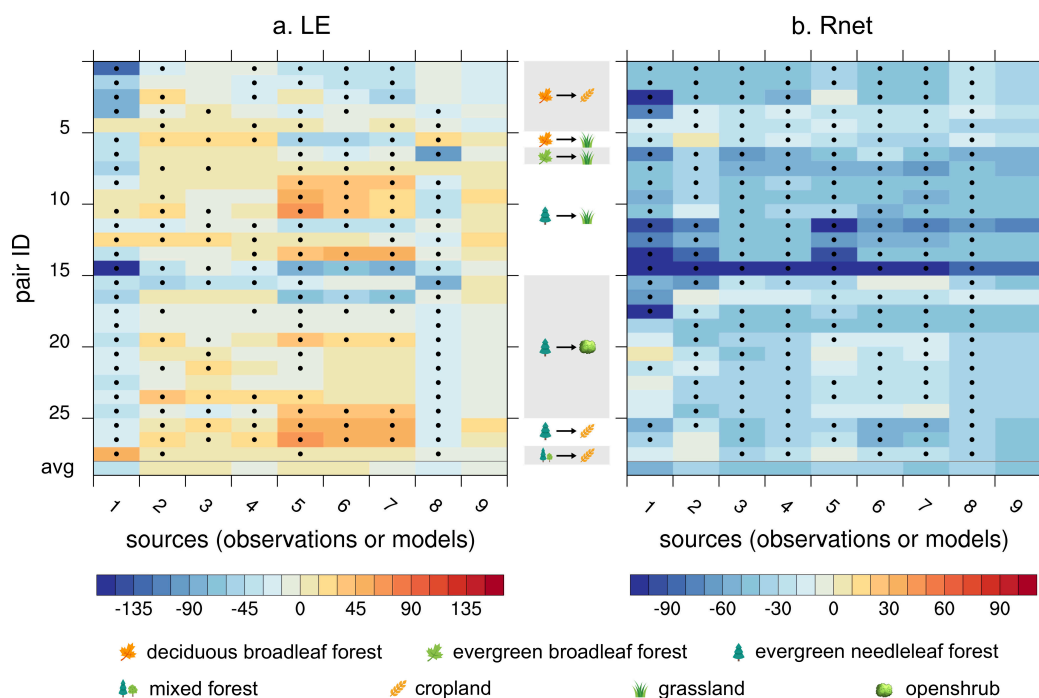


697

698 **Figure 10.** Same as Figure 4 but for R_{net} (W/m^2).

699

700

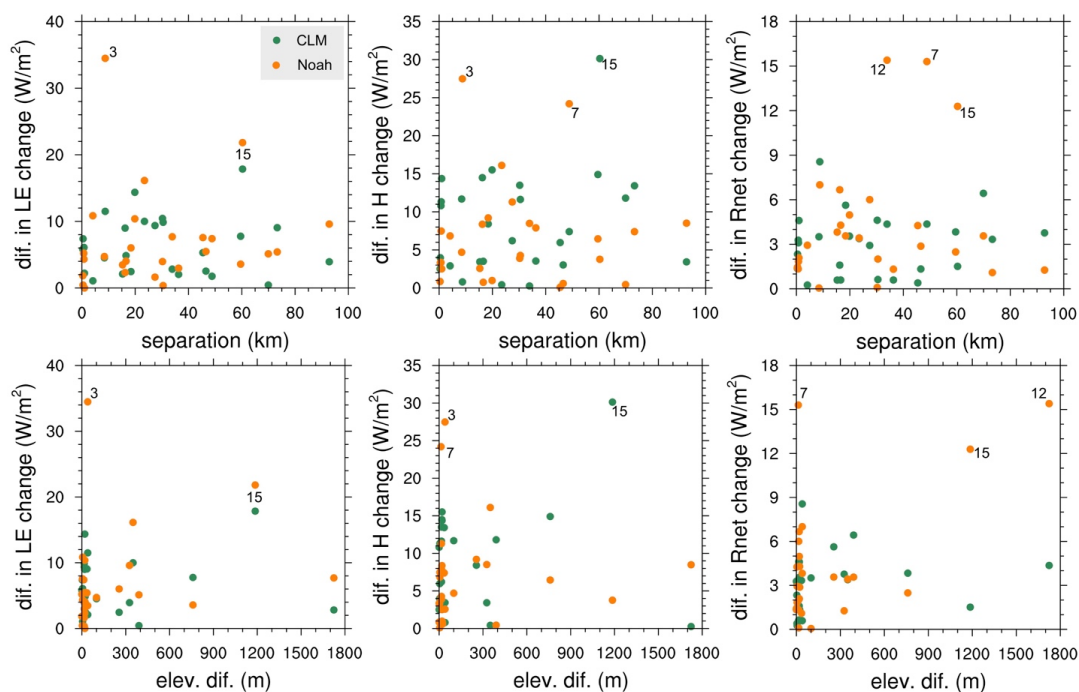


701

702 **Figure 11.** Change in observed and simulated LE (a) and R_{net} (b) during summer daytime
 703 (averaged during the period 08:00 ~ 16:00) over individual pairs and their averages. The
 704 horizontal labels show the sources: 1. FLUXNET_MDS; 2. CLM; 3. CLM_forest; 4.
 705 CLM_open; 5. NOAH-MP; 6. NOAH-MP_forest; 7. NOAH-MP_open; 8. CLM-PFT; 9. CLM-
 706 PFTCOL. The vertical labels show the pair ID from 1 to 28 based on Table S1. The pairs are
 707 grouped based on the type of LULCC (shown as the icons in the middle). The bottom row is the
 708 average over all pairs. The Student's t-test is performed on the daily (daytime average) time
 709 series for each pair. Dots indicate statistically significant changes at the 95% confidence level.
 710 No significant test is carried out for the CLM-PFTCOL simulation (the last column), because we
 711 only have long-term averaged hourly output for each month.

712

713



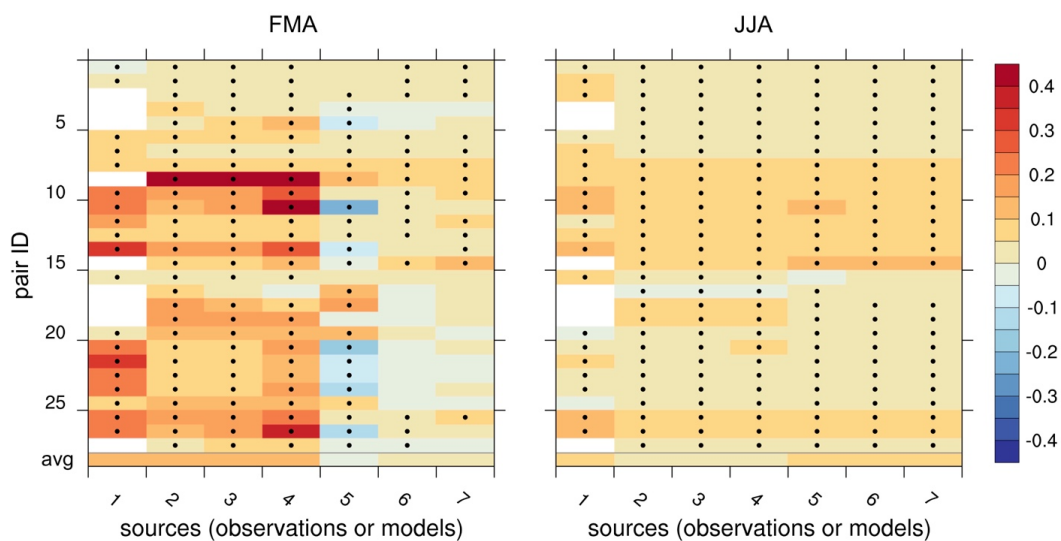
714

715 **Figure 12.** Sensitivity of differences in simulated surface energy flux changes (left column: *LE*,
 716 middle: *H*, and right: *R_{net}*) between “forest forcing” and “open forcing” simulations to site
 717 separation (top) and elevation difference (bottom) between the forest and open sites in individual
 718 pairs. The pairs No. 3, 7, 12 and 15 are labeled because of the greatest differences in surface
 719 fluxes changes.

720

721

722



723

724 **Figure 13.** Same as Figure 11, but for the change in observed and simulated daytime albedo

725 during late winter/early spring (FMA, left) and summer (JJA, right). The horizontal labels show

726 the sources: 1. FLUXNET_MDS; 2. CLM; 3. CLM_forest; 4. CLM_open; 5. NOAH-MP; 6.

727 NOAH-MP_forest; 7. NOAH-MP_open. White areas indicate missing observations.

728